Turbulence in the Evolving Stable Boundary Layer

S. J. CAUGHEY[1]

Meteorological Research Unit, RAF Cardington, England

J. C. WYNGAARD

Cooperative Institute for Research in Environmental Sciences, University of Colorado/NOAA, Boulder 80309, and Wave Propagation Laboratory, NOAA/ERL, Boulder, CO 80302

J. C. KAIMAL

Wave Propagation Laboratory, NOAA/ERL, Boulder, CO 80302

(Manuscript received 7 November 1978, in final form 13 February 1979)

ABSTRACT

The turbulence structure observed in seven early evening runs of the 1973 Minnesota experiments is presented and discussed. Wind and temperature sensors mounted on a 32 m tower and on the tethering cable of a large balloon spanned the entire depth of the rapidly evolving nocturnal boundary layer. Spectral shapes and the vertical profiles of turbulence variances and covariances, dissipation rates for turbulent kinetic energy and temperature variance, and energy-containing range length scales show remarkable order when plotted in dimensionless coordinates, even though properties varied widely among the runs. Observed dissipation rates and boundary layer depth agree well with predictions of the Brost-Wyngaard (1978) model. It is shown that the slight (0.0014) terrain slope and possibly baroclinity affected the boundary-layer evolution, and that although the turbulence structure was probably in equilibrium with the wind and temperature fields, these were strongly evolving during the runs.

1. Introduction

Our understanding of the structure of the atmospheric boundary layer (ABL) has made significant strides in recent years with progress on both theoretical and experimental fronts. The Minnesota 1973 experiment (Readings *et al.*, 1974; Kaimal *et al.*, 1976) provided some insight into the behavior of convective boundary layers and demonstrated the validity of mixed-layer scaling for heights in the range 0.1 z_i to 0.9 z_i, where z_i is boundary-layer depth. Those findings have been augmented by further studies by Caughey and Kaimal (1977), Panofsky *et al.* (1977), Caughey and Wyngaard (1979), Jensen and Lenschow (1978), Kaimal (1978) and Panofsky (1978), and the numerical modeling work of Deardorff (1973a, 1973b, 1974a, 1974b) and Arya and Wyngaard (1975).

The stable boundary layer, on the other hand, presents a more challenging problem since stationary and horizontal homogeneity conditions are seldom satisfied. Data for stable conditions are more sparse, but increased understanding has been gained through model studies. Businger and Arya (1974) calculated some of the important features of an idealized, steady-state case, while Delage's (1974) model study revealed aspects of the behavior of evolving stable boundary layers. Using a higher order closure model Wyngaard (1975) was able to simulate the evolution of the nocturnal boundary layer and found good agreement with observations made during the Minnesota experiment. Further work by Brost and Wyngaard (1978) has emphasized the important role typically played by the surface energy budget and terrain slope in nocturnal boundary-layer evolution. In this paper we will examine data obtained during the Minnesota experiment to study further the evolving nocturnal boundary layer.

The Minnesota 1973 experiment was a joint venture by the Air Force Cambridge Research Laboratories[2] (AFCRL) at Bedford, Massachusetts, and the Meteorological Research Unit (MRU) at RAF Cardington, England. Details of the experiment and the characteristics of the site can be found in earlier papers by Readings *et al.* (1974) and Kaimal *et al.* (1976). Briefly, the experiment was conducted over nearly flat terrain to investigate the structure of the entire boundary layer. Measurements of wind and temperature fluc-

[1] Present affiliation: Meteorological Office, Bracknell, Berks., England.

[2] The laboratory has since been renamed Air Force Geophysics Laboratory.

0022-4928/79/061041-12$07.00

TABLE 1. List of runs and significant boundary-layer parameters.

Run	Date (1973)	Period (CDT)	$-Q_0$ (K m s^{-1})	u_* (m s^{-1})	T_* (K)	L (m)	h (m)	$(\mathrm{Ri})_{4m}$	$(z/L)_{4m}$
1B2	6 Sep	1916–2031	0.0082	0.16	0.051	43	210	0.086	0.093
2C2	10 Sep	1850–2005	0.0217	0.31	0.070	116	400	0.022	0.034
2D1	10 Sep	2012–2127	0.0130	0.13	0.100	14	90	0.085	0.29
3B2	11 Sep	1905–2020	0.0120	0.21	0.057	66	320	0.046	0.061
5B1	15 Sep	1902–2017	0.0047	0.12	0.039	31	110	0.095	0.13
5B2	15 Sep	2017–2132	0.0045	0.06	0.074	4.4	30	0.16	0.91
7E1	19 Sep	1935–2050	0.0064	0.10	0.064	13	100	0.10	0.31

tuations were made at two levels (4 and 32 m) on a 32 m tower with AFCRL's three-component sonic anemometers and fine platinum wire thermometers. Profiles of mean wind and temperature were obtained from logarithmically spaced sensors on the tower. Five MRU turbulence probes attached at heights ranging from 61 to 1219 m to the tethering cable of a large captive balloon extended the tower measurements to heights well above the surface inversion. The turbulence probe heights varied from run to run and since the runs examined here were continuations of those started during the day, the spacing of the probes on the tethering cable had been chosen for best coverage in the convective boundary layer. As a result, some of the upper levels were not particularly useful for this study. Nevertheless, the seven selected runs containing a total of 22 discrete observation heights provide sufficient data for dimensionless plots of turbulence parameters.

Data collection was restricted to periods when the winds were northerly, the direction in which the tower sensors were pointed. The runs were terminated around midnight when conditions often became unsuitable for operation; typically the winds became southerly or the turbulent activity at 4 m subsided altogether.

2. Description of the data

The runs listed in Table 1 fall within the period between onset of negative heat flux (we call this "transition") and cessation of turbulence near the surface. Time histories of temperature, vertical temperature flux and friction velocity at 4 m are shown in Fig. 1 and illustrate the nonstationary nature of the periods. The plots were constructed from 15 min averaged data centered over the averaging period.

All parameters listed in Table 1 are averages over 75 min periods. Q_0 is the surface temperature flux approximated by $\overline{w\theta}$ at 4 m, u_* is the friction velocity approximated by $(-\overline{uw})^{\frac{1}{2}}$, also at 4 m, while T_* is the scaling temperature defined as $-Q_0/u_*$. The Obukhov length L follows the standard definition,

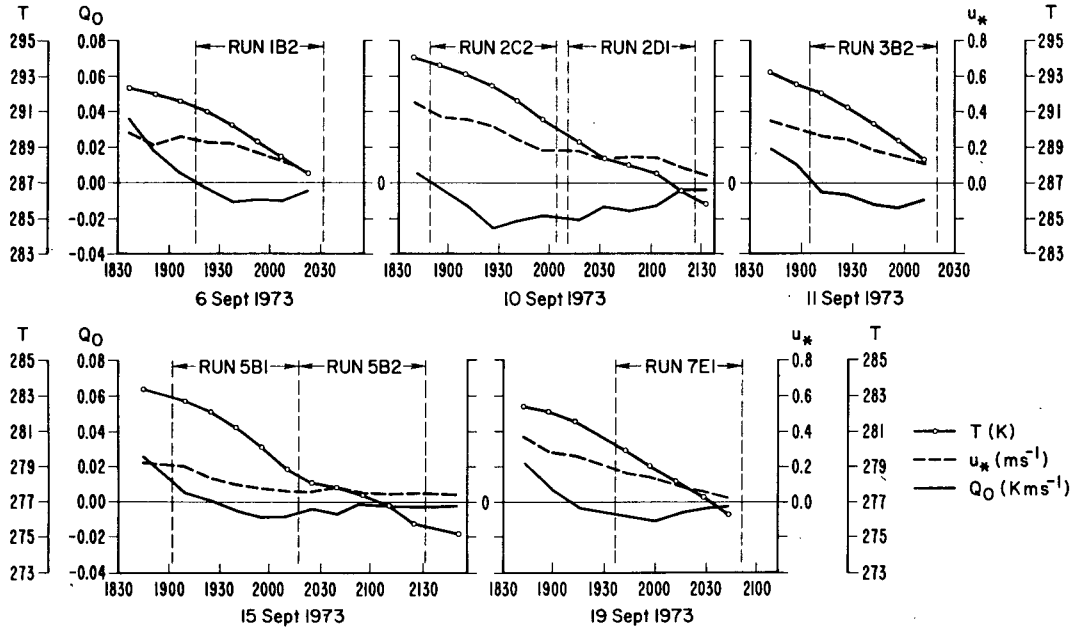

FIG. 1. Time histories showing variation of 1 m temperature, u_* and Q_0 for the runs used in analysis presented here. Each data point represents a 15 min average.

while the boundary-layer depth h is taken as the height at which the vertical temperature flux falls to 5% of its surface value. The surface temperature flux values are typically an order of magnitude smaller than the midafternoon values reported by Kaimal *et al.* (1976) for these days. Table 2 provides information on the observation heights for each run and the dimensionless heat flux at each level.

The variances and fluxes given in the tables are not computed directly from the time series but estimated by integrating the spectral and cospectral curves over the bandwidth 0.001–5 Hz. This approach reduced contributions from long-term trends or wave motions (Caughey and Readings, 1975) which appear as a secondary peak at the low-frequency end. This secondary peak is also observed at the same frequency above the boundary layer, while the primary peak representing turbulent activity in the boundary layer disappears there. Similar behavior has been observed by Caughey (1977) in stable spectra recorded over a much less homogeneous site. The variances and covariances obtained through integration over the frequency band $0.001<n<5$ Hz differed very little at 4 m height from estimates computed directly from the time series, but departed appreciably at the upper levels presumably due to the relatively larger contribution in the time-averaged quantities from the secondary peak.

TABLE 2. Profiles of turbulence parameters

Run	z (m)	z/h	$-\overline{w\theta}/u_*T_*$	σ_w^2/u_*^2	σ_θ^2/T_*^2
1B2	4	0.02	1.00	2.20	4.57
	32	0.15	0.58	1.70	2.27
	61	0.29	0.19	0.96	0.96
2C2	4	0.01	1.00	1.96	5.46
	32	0.08	0.86	*	3.82
	61	0.15	0.46	1.39	2.14
	305	0.76	0.08	0.63	0.23
2D1	4	0.04	1.00	2.10	4.04
	32	0.36	0.37	0.96	1.81
	61	0.68	0.12	0.67	0.53
3B2	4	0.01	1.00	2.30	5.63
	32	0.10	0.88	2.00	4.93
	61	0.19	0.41	1.60	1.79
	152	0.48	0.24	*	0.46
	305	0.95	0.10	*	0.25
5B1	4	0.04	1.00	2.0	7.40
	32	0.29	0.23	1.5	1.24
	61	0.55	0.13	1.18	0.32
5B2	4	0.13	1.00	1.90	4.20
7E1	4	0.04	1.00	1.95	4.20
	32	0.32	0.22	*	0.90
	61	0.61	0.20	1.2	0.30

* Denotes spectrum not suitable for integration.

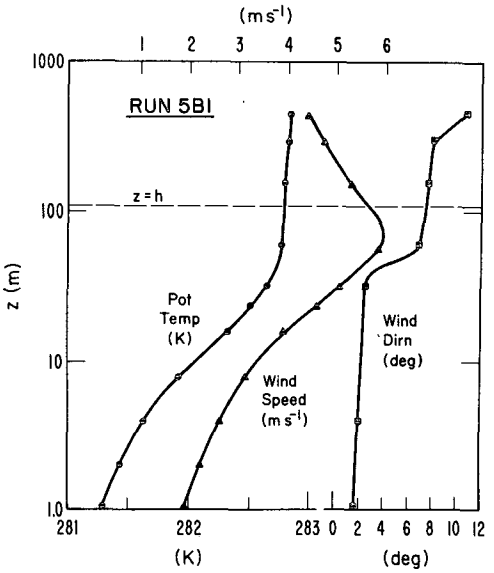

FIG. 2. Typical mean profiles of wind speed, wind direction and potential temperature showing their relationship to boundary-layer depth h.

It should also be recognized that the values in Tables 1 and 2 are averages obtained during periods when the surface temperature and wind speed were falling rapidly and the fluxes themselves were varying with time. In particular, the h values represent no more than an average boundary-layer depth; note the change in h between consecutive periods in runs 2 and 5. Fig. 2 shows how the estimated h relates to the wind and temperature profiles for one of the runs in Table 1.

Absent from the tables are the turbulence statistics involving the lateral component v. The effect of balloon movement (Kaimal *et al.*, 1976) on the v spectra was too severe to justify any analysis other than estimation of the wavelength at the spectral peak for comparison with the longitudinal u and vertical w spectral peaks.

3. Observed turbulence structure

a. Spectra and cospectra

In analyzing the Minnesota data we followed the approach used by Kaimal (1973) and Caughey (1977) which demonstrated the universal nature of spectra and cospectra in the lower layers of a stable boundary layer. Logarithmic spectral and cospectral estimates normalized by their integral over the frequency band of interest were plotted as a function of f/f_0, where f is the reduced frequency $(=nz/U\approx z/\lambda)$ and f_0 the reduced frequency at the intercept of the extrapolated inertial subrange with an ordinate value of unity. This formulation forced the different spectra and cospectra to collapse into single curves in the inertial subrange; since the overall shape of the individual

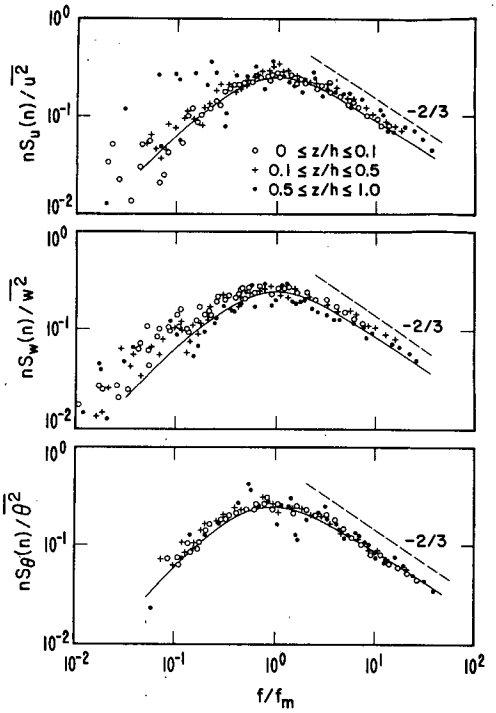

FIG. 3. Normalized logarithmic spectra of u, w and θ plotted against f/f_m. Curves are from the Kansas data (Kaimal, 1973).

curves varied little with height and stability, the fit remained good over the entire bandwidth. Simple interpolation formulas for these curves were obtained and expressions relating f_0 and λ_m, the wavelength at the spectral and cospectral maximum, were derived empirically as functions of Richardson number Ri.

We have made two departures from the previous studies in our choice of variables here: f_0 is replaced by f_m, the reduced frequency at the spectral (or cospectral) peak and Ri is replaced by dimensionless height z/h as the independent variable for plotting turbulence quantities. The changes were necessary to accommodate possible departures from the simple relationships found in the surface layer and to explore the influence of boundary-layer depth on the spectral and cospectral scales.

The relationship between f_0 and f_m is obtained directly from the spectral and cospectral forms of Kaimal (1973)

$$f_0 = \begin{cases} 0.26 f_m & \text{(for } u, v, w \text{ and } \theta) \\ 1.27 f_m & \text{(for } uw \text{ and } w\theta) \\ 1.39 f_m & \text{(for } u\theta). \end{cases} \quad (1)$$

Substituting for f_0 in the formulas gives the curves shown in Figs. 3 and 4. The secondary peaks which occur roughly two decades below the main peak f_m are not shown in the plots. To further minimize confusion only three sets of spectral and cospectral estimates from each z/h category are shown in the plots, but their behavior is typical of other runs in their respective categories. The best agreement is seen in the u and θ spectra (except for u above $0.5h$). The w spectra at all heights show more energy on the low-frequency side compared to the Kansas spectra. This tendency was observed in the unstable spectra as well (Kaimal, 1978) for reasons yet unclear. In general, there is more scatter in the cospectral plots at $z>0.1h$. Not surprisingly, uw fares worse than either $w\theta$ or $u\theta$, with occasional positive values (not shown in the plot) at the low-frequency end. The normalized intensity at the peak is approximately the same for all the plots. The average value for u, w and θ varies between 0.25 and 0.26, and for uw, $w\theta$ and $u\theta$, between 0.28 and 0.29.

The dimensionless coordinates of Figs. 3 and 4 mask any height dependence that might exist in the spectral intensities and in the predominant wavelength λ_m. We find that a consistent pattern does emerge when these parameters are plotted against z/h (see Figs. 5, 6 and 7). Faired curves drawn through the dimensionless variances and covariances approach zero at $z/h=1$. The sharpest drops with height are seen in $\overline{\theta^2}$ and $\overline{w\theta}$, which fall to one-tenth their surface values in the first half of the boundary layer. The variances of u and w drop more slowly, but there is considerably less scatter in u than in w. This is a shift from observed daytime behavior where w statistics scatter significantly less than u. Of the three covariances, $\overline{uw}$ has the most scatter but that comes as no surprise.

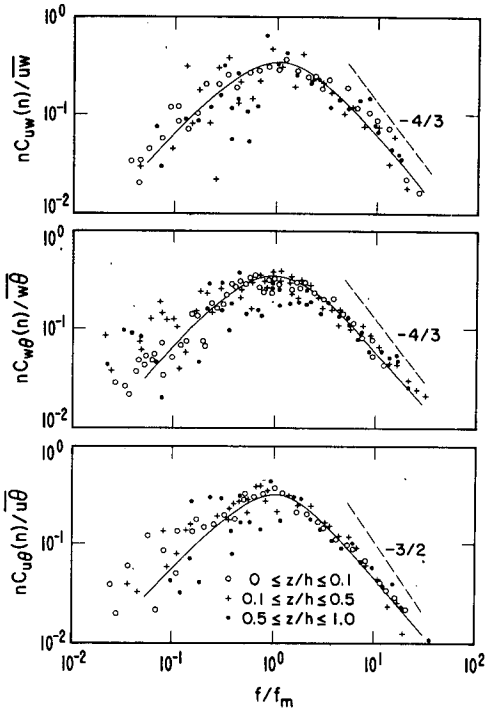

FIG. 4. Normalized logarithmic cospectra of uw, $w\theta$ and $u\theta$ plotted against f/f_m. Curves as in Fig. 3.

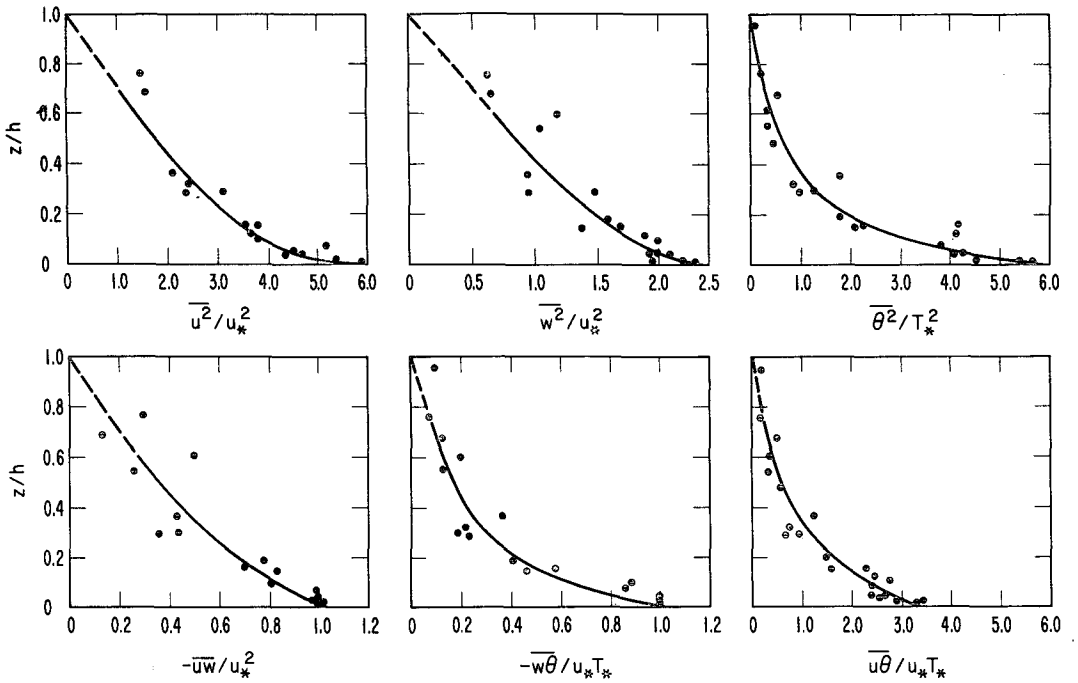

FIG. 5. Vertical profiles of dimensionless variances and covariances.

The sets of data plotted in Figs. 6 and 7 collapse remarkably well considering the fact that the boundary-layer depth was varying with time. Near the surface ($z<0.1h$), the peak wavelength is different for each variable; λ_m values are longest for u and θ and smallest for w. Despite these differences there exists a distinct tendency for λ_m/h in all plots to approach unity at the top of the boundary layer; only θ and $u\theta$ indicate somewhat larger values.

In order to represent the Kansas formulas (Kaimal, 1973) for the different λ_m's (expressed originally as linear functions of z/Ri) in the coordinates of Figs. 6 and 7, we used the Kansas relation between Ri and z/L (Businger *et al.*, 1971), i.e.,

$$\mathrm{Ri}=\frac{[0.74+4.7(z/h)(h/L)](z/h)(h/L)}{[1+4.7(z/h)(h/L)]^2}, \qquad 0\leqslant z/L\leqslant 2, \quad (2)$$

where we have written $z/L=(z/h)(h/L)$. Fig. 8, a plot of Ri vs z/h for the Minnesota data, is a test of (2). The curves in Fig. 8 are the predictions of (2) for $h/L=3$ and 8, since the Minnesota data (Table 1) fall between these extremes. Fig. 8 shows that the curves do bracket most of the experimental points, implying close agreement between the Kansas and Minnesota data.

The Kansas λ_m formulas, converted with (2) for $h/L=3$ and 8, are shown as dashed lines in Figs. 6 and 7. The Kansas data were taken at heights of 23 m and below, and h was not measured, so we have

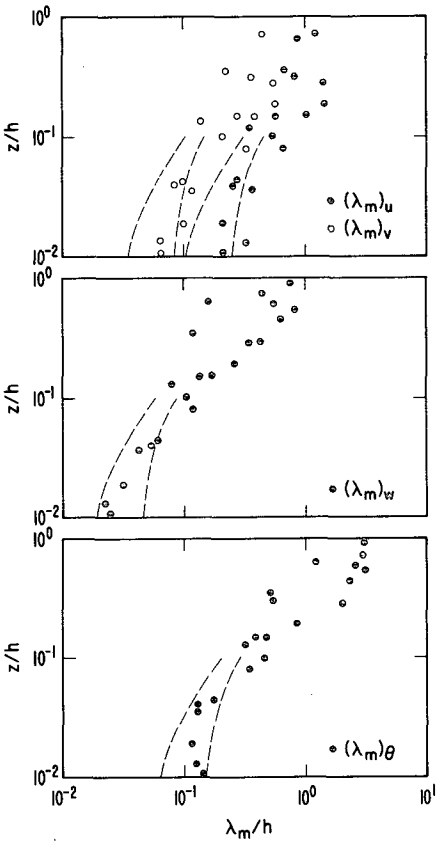

FIG. 6. Vertical profiles of λ_m for u, v, w and θ. Curves are from the Kansas data (Kaimal, 1973) for $h/L=3$ and 8, the range of the present data.

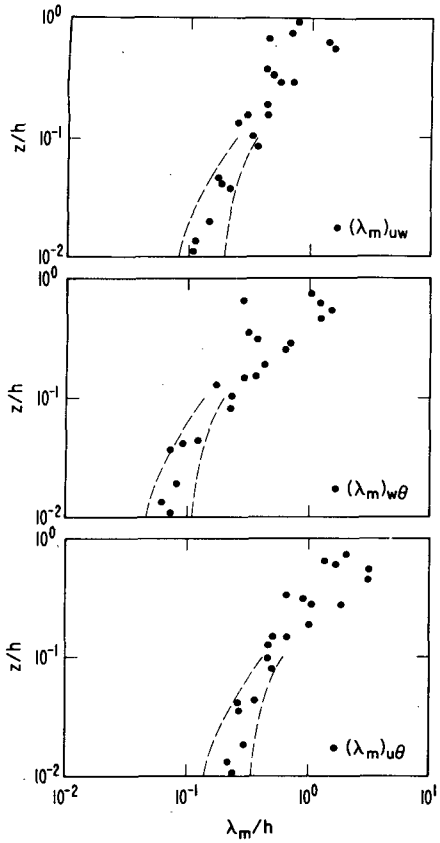

FIG. 7. Vertical profiles of λ_m for uw, $w\theta$ and $u\theta$. Curves as in Fig. 6.

arbitrarily stopped the curves at $z=0.1h$. Figs. 6 and 7 show that the Minnesota λ_m/h values for $z<0.1h$ are in good agreement with the Kansas results.

b. Dissipation rates and structure parameters

Dissipation rates ϵ and N, for the turbulent kinetic energy and one-half the temperature variance, respectively, are plotted in dimensionless forms in Fig. 9.

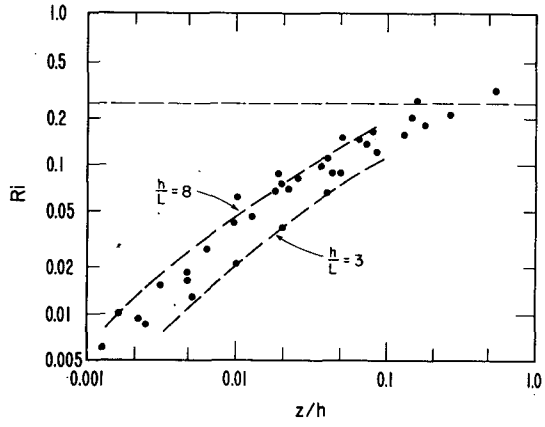

FIG. 8. Richardson number at 4 and 32 m plotted as a function of z/h. Curves are from the Kansas data (Businger *et al.*, 1971).

They were estimated from the inertial subrange spectral levels of w and θ as described by Kaimal *et al.* (1972). Both ϵ and N decrease with height, somewhat gradually in the lower layers ($0.001h<z<0.1h$) and more rapidly above $0.1h$. Fig. 9 also includes dimensionless plots of the structure parameters C_v^2 and C_T^2, which are related to ϵ and N by (Kaimal, 1973):

$$C_v^2=2\epsilon^{\frac{2}{3}}, \tag{3}$$

$$C_T^2=3.2N\epsilon^{-\frac{1}{3}}. \tag{4}$$

The Kansas results (Wyngaard and Coté, 1971) show that the turbulent flux divergence (transport) terms in the budgets of turbulent kinetic energy and temperature variance are negligible in the stable surface layer. To a good approximation this implies that

$$\epsilon=-\overline{uw}\frac{\partial U}{\partial z}+\frac{g}{T}\overline{\theta w}, \tag{5}$$

$$N=-\overline{\theta w}\frac{\partial \Theta}{\partial z}, \tag{6}$$

where Θ is the mean potential temperature. Nondimensionalizing (5) and (6) and using the Kansas results for $\partial U/\partial z$ and $\partial\Theta/\partial z$ (Businger *et al.*, 1971) gives

$$\frac{\epsilon h}{u_*^3}=\frac{1}{k}\frac{[1+3.7(z/h)(h/L)]}{(z/h)}, \tag{7}$$

$$\frac{Nh}{u_*T_*^2}=\frac{1}{k}\frac{[0.74+4.7(z/h)(h/L)]}{(z/h)}. \tag{8}$$

Eqs. (7) and (8) are shown as dashed curves in Fig. 9 for $k=0.35$, $h/L=3$ and 8, and $z\leqslant 0.1h$. Although there is some scatter, (7) and (8) are a reasonable representation of the surface-layer data from Minnesota as well.

The solid curves in Fig. 9 are based on the model calculations of Brost and Wyngaard (1978), who studied the evolution of a nocturnal boundary layer. The curves shown are for a near-surface cooling rate of 4 K h^{-1}, which is close to the average value of 3.6 K h^{-1} at $z=1$ m observed in Minnesota for the first 2 h after transition. The midpoints of the Minnesota runs (Fig. 1) occurred, on average, about 1 h after transition, but because of rapid transient response and possible sensitivity to initial conditions we considered the model results only after 2 or more hours. Nonetheless, the model results for ϵ and N at 2 h (Fig. 9) agree quite well with the Minnesota data. The model results indicate that if the cooling rate is sustained, the ϵ and N profiles above the surface layer continue to evolve for several hours.

c. Boundary-layer depth

Zilitinkevich (1972) predicted that the dimensionless depth hf/u_* of the idealized, steady, stably stratified

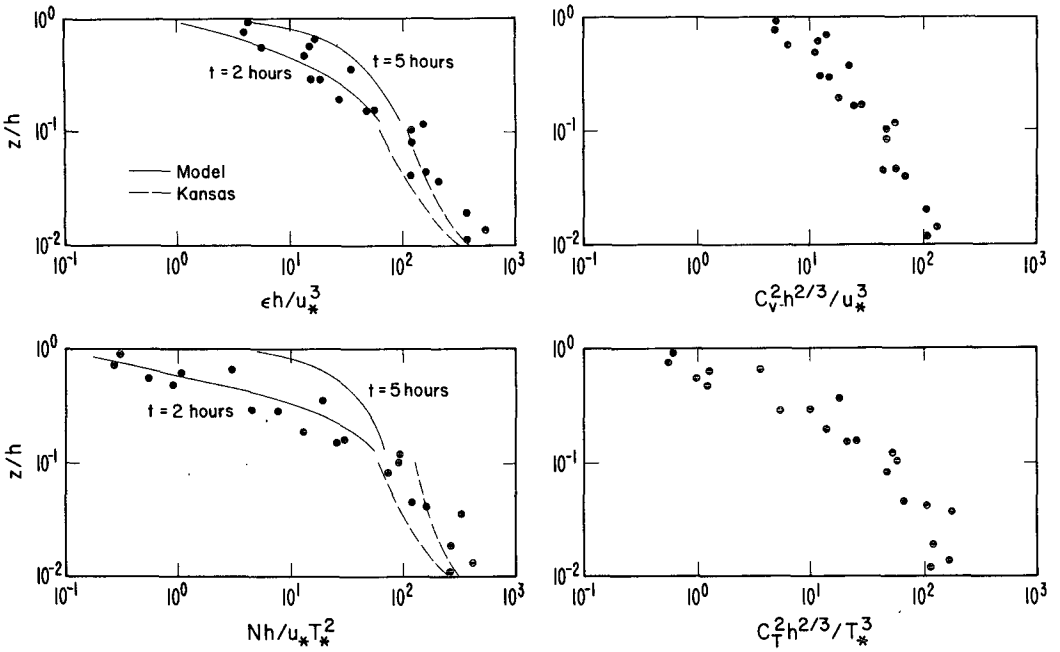

FIG. 9. Vertical profiles of dimensionless dissipation rates and structure parameters. Solid curves are from the Brost-Wyngaard (1978) model calculations of ϵ and N for two times after transition, for a near-surface cooling rate of 4 K h^{-1}; dashed curves are from Kansas data [Eqs. (7) and (8)] for $h/L=3$ and 8.

ABL behaves as

$$\frac{hf}{u_*}=d\left(\frac{u_*}{fL}\right)^{-\frac{1}{2}}, \tag{9}$$

where f is the Coriolis parameter and d a universal constant. Although our h values decreased substantially with time, we have plotted in Fig. 10 the average value for each run in the form suggested by (9). The results are seen to be consistent with (9), and also with the Brost-Wyngaard model at 2 h; the line in Fig. 10 at 2 h corresponds to $d=0.7$. According to this model, d decreases and approaches 0.4 as the ABL approaches steady state.

4. Evolution of the stable boundary layer

As we made clear in the previous discussions, the boundary layer was rapidly evolving in the evening Minnesota runs. In this section we discuss first some of the factors influencing this evolution, and then examine in more detail some of its effects on boundary-layer structure.

a. Influences

While the marked changes with time in Fig. 1, for example, are largely due to the transition from unstable to stable stratification in the surface layer, there is evidence that synoptic conditions and local terrain effects also had some influence.

The surface and 850 mb weather maps show synoptic features common to all of the runs. The tower boom orientation restricted us to runs with northerly winds, and these tended to be associated with high-pressure ridges moving in from the northwest. These systems moved rather rapidly, usually giving no more than 24 consecutive hours of suitable winds; in addition, the pressure gradient and hence the wind speed tended to decrease steadily as the ridge approached.

As discussed by Wyngaard (1975), we estimated G, the surface geostrophic wind speed, using surface

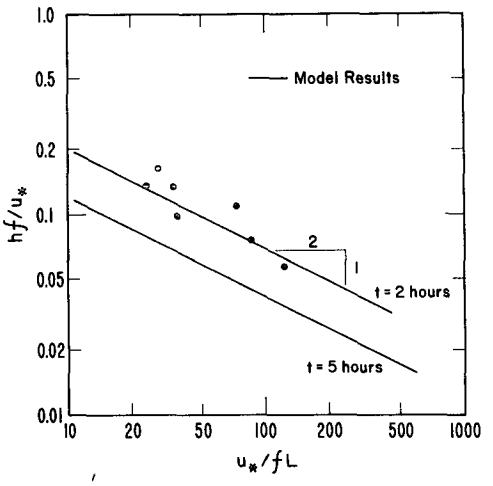

FIG. 10. A test of the similarity prediction (9) for ABL depth h. Solid curves are from the Brost-Wyngaard (1978) model for a near-surface cooling rate of 4 K h^{-1} at 2 and 5 h after transition.

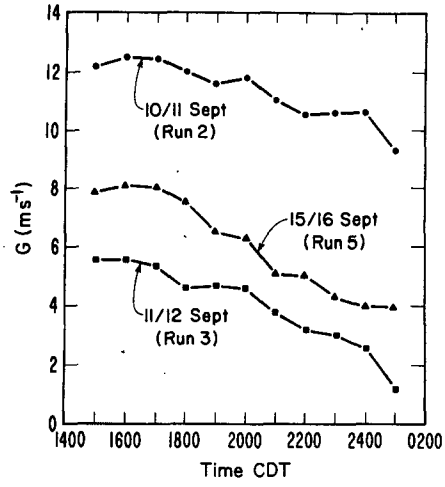

FIG. 11. Time variation of surface geostrophic wind G for periods covering runs 2, 3 and 5.

pressure data from local NWS surface stations. We used two data sets, each based on four stations; one set had N–S, E–W orientations, the other NE–SW, NW–SE. Station separations varied from 350–580 km, with the tower near the array center. The G results, averaged over the two data sets, are shown in Fig. 11. While surface pressure fields were not available for all runs, judging from the surface maps the steady decrease in G seen in Fig. 11 is typical. Note that in the 34 h period between 1500[3] 10 September to 0100 on 12 September, G decreased from about 12 m s^{-1} to 1 m s^{-1}. The trend in surface geostrophic wind direction was much weaker, tending to rotate slightly clockwise (CW) with time.

The surface and 850 mb maps show that the horizontal mean pressure gradient varied substantially within a 500 km radius of the tower in some of the runs. This is a variation of sufficiently small scale that advection could have been significant in the boundary-layer mean momentum balance. The maps also suggest that this pressure gradient typically varied significantly between the surface and the 850 mb level (~1200 m above the surface). Thus the ABL flow was probably baroclinic, which is also suggested by the strongly curved stress profiles in the daytime, as discussed by Kaimal *et al.* (1976).

It is well-established that terrain slope can influence nocturnal ABL evolution since it creates a drainage acceleration. Fig. 12 shows, on an expanded vertical scale, the terrain on a 13 km×16 km area surrounding the tower. Although the N–S slope is nearly zero over this region, there is a persistent upward slope to the east; at the tower, this slope magnitude is about 0.0014. We will show later that this leads to a significant drainage acceleration when the near-surface air cools.

The dominant influence on nocturnal ABL evolution is the stable stratification. Given the same mean pressure gradient, a stably stratified ABL supports less stress than a neutral or convective one; this is the principal reason for the decay in u_* shown in Fig. 1. Immediately after transition the heat flux rapidly grows, but in conjunction with the falling u_* value this creates increasingly stronger stable stratification. Thus the heat flux soon reaches a negative maximum, and then tends to decrease in magnitude as the stability limits the turbulent heat transfer. Fig. 13 clearly shows the details of this process at 4, 32 and 61 m during run 2. Note from Fig. 13 that after the rapid buildup phase the ABL depth, as judged by the (extrapolated) height where heat flux vanishes, decreases with time.

b. The surface wind direction and the Ekman spiral

The evolution of ABL properties shown in Fig. 1 is consistent with that predicted over a horizontal surface under barotropic conditions (e.g., Delage, 1974; Wyngaard, 1975; Brost and Wyngaard, 1978). However, other properties do show some unexpected trends. Consider, for example, the near-surface wind direction α. In an idealized (quasi-steady, barotropic, horizontally-homogeneous) ABL, the angle between surface and geostrophic winds (the cross-isobaric angle) is smallest under convective conditions, larger

[3] All times CDT.

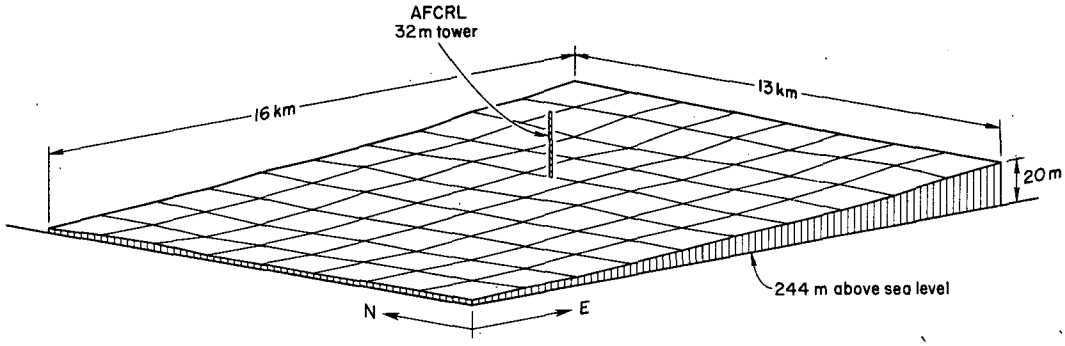

FIG. 12. Terrain slope at the Minnesota site shown in exaggerated vertical scale. Grid size for this plot corresponds to square mile sections on U.S. Geological Survey topographical maps.

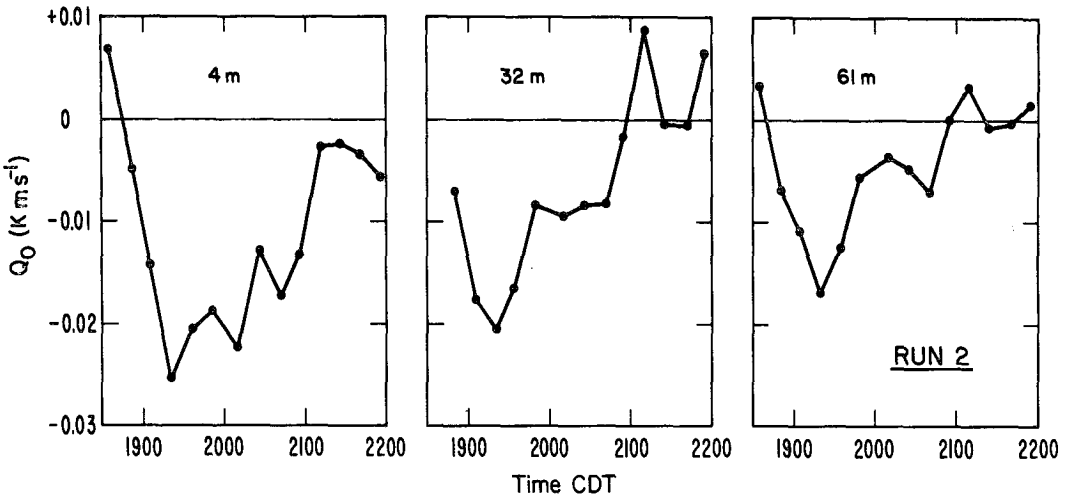

FIG. 13. Time variation in the vertical temperature flux at different heights during run 2.

at neutral and largest under stable conditions; the range runs from a few degrees to roughly 45°. Thus during transition under idealized conditions we should expect the cross-isobaric angle to increase in response to the increasing stability, and (in the Northern Hemisphere) the surface wind to rotate counterclockwise (CCW).

In fact, we observed CCW rotation of surface winds after transition only in runs 2 and 5; in the other three runs the rotation was CW. Fig. 14 shows the evolution of wind direction in "normal" (run 2) and "abnormal" (run 3) cases. Note that in run 2, the 4 m wind began rotating CCW at about the time of transition. In run 3, by contrast, the wind at 4, 61 and 457 m rotates CW, giving a "backward" Ekman spiral; runs 1 and 7 behaved similarly.

Neumann (1977) has derived an equation expressing the time evolution of mean wind direction, and we can easily extend it to include the drainage accelerations caused by terrain slope. We assume a flat but slightly inclined surface and choose horizontal coordinates x and y parallel to it, denoting the horizontal mean wind vector by (U,V). We assume the boundary-layer depth does not vary with x or y, so the usual mean momentum equations, with an added drainage acceleration term, apply (Brost and Wyngaard, 1978). Defining $\alpha=\arctan(V/U)$, and noting that

$$\dot{\alpha}=\frac{\partial\alpha}{\partial t}=\frac{1}{S^2}(U\dot{V}-V\dot{U}), \tag{10}$$

where $S^2=U^2+V^2$, allows the α equation to be developed from those for U and V. The result is

$$\left.\begin{aligned}\dot{\alpha}=&-U_i\frac{\partial\alpha}{\partial x_i} && \text{(advection)}\\ &+\frac{1}{S^2}\left(V\frac{\partial}{\partial z}\overline{uw}-U\frac{\partial}{\partial z}\overline{vw}\right) && \text{(friction)}\\ &+f\left(\frac{G}{S}\cos\gamma-1\right) && \text{(pressure-Coriolis)}\\ &+\frac{g}{T_0}\frac{\bar{T}'}{S^2}(V\beta_x-U\beta_y) && \text{(drainage)}\end{aligned}\right\}. \tag{11}$$

Here γ is the angle between the geostrophic and mean winds, T_0 is the reference adiabatic temperature (Lumley and Panofsky, 1964), which we take as the temperature above the boundary layer, $\bar{T}'=T-T_0$ is the deviation from this adiabatic temperature, and β_x and β_y are the x and y components of the terrain slope vector. We will call (11) the α budget.

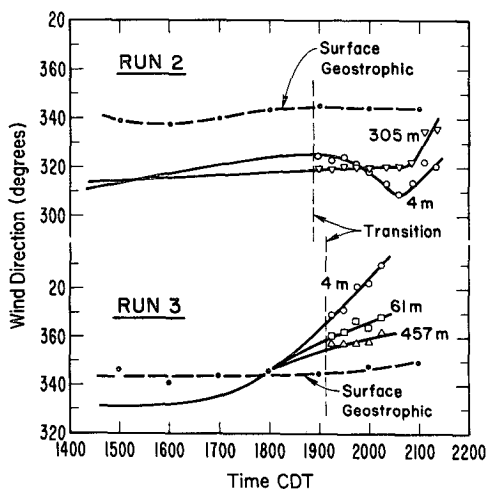

FIG. 14. Change in wind direction at different heights, following transition to stable lapse rates, compared to surface geostrophic wind. Note reverse Ekman spiral in run 3.

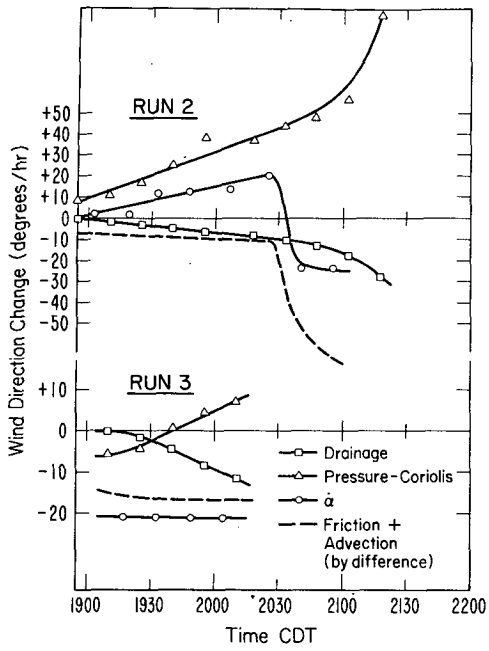

FIG. 15. Contributions from terms in the α budget shown as a function of time for runs 2 and 3.

The α budget can be interpreted very simply under steady conditions over a horizontally homogeneous, zero-slope surface in a given hemisphere, say northern. Then the friction and pressure-Coriolis terms balance; further, $(G/S)\cos\gamma > 1$, so the pressure-Coriolis term is positive and the friction negative. The negative friction in this case can also be simply explained: due to the Ekman spiral, the faster, upper level winds are rotated CW with respect to the surface layer winds, giving a CW (negative) frictional acceleration in the surface layer due to this angular shear.

During transition in this idealized case, turbulent friction causes S to decrease, which in turn increases the pressure-Coriolis term. The friction term also changes, but the pressure-Coriolis term dominates and α rotates CCW. This simple picture can change in a baroclinic PBL (where the pressure-Coriolis term can be larger or smaller) or over sloped terrain.

The drainage term in the α budget vanishes when the wind and slope vectors are parallel, and is largest when they are perpendicular; the latter condition is closer to the Minnesota situation. Thus even though the slope angle β was small (~ 0.0014) the drainage term at $z=4$ m became important during the mid-stages of each of our runs. It was always negative, with magnitude becoming of the order of f or larger in runs 1B2, 2D1, 5B1, 5B2 and 7E1.

Since we had some data on surface geostrophic wind, we could compute the α budget at 4 m for some runs. Results for runs 2 and 3 are shown in Fig. 14. Note that $\dot{\alpha}$ was positive for most of run 2, due to the strong pressure-Coriolis term. The friction-advection (obtained by difference) and drainage terms acted in opposition to the pressure-Coriolis terms. Fig. 14 shows that immediately after transition in run 2 the wind direction shear between 4 and 305 m is not of the expected sign, given the negative friction, but the wind direction profile in this period had unusually large scatter. Later, however, the expected direction shear developed. The strong change in $\dot{\alpha}$ between 2020 and 2035, also evident in Fig. 14, is evidently due to a corresponding jump in friction or advection.

Run 3 behaves quite differently according to Fig. 15. Here $\dot{\alpha}$ is strongly negative and much larger in magnitude than the pressure-Coriolis term. Evidently friction (which has a sign consistent with the observed direction shear) or advection is primarily responsible for this unusual behavior, but the drainage term is also large. The abnormally small pressure-Coriolis term could have been due to baroclinity. Arya and Wyngaard (1975) have argued that the mean wind in a convectively mixed layer responds to the layer-averaged G; however, in late afternoon as convection decays the well-mixed character is lost, and the turbulent friction can no longer support the large local geostrophic departure. Thus an acceleration develops, but in the meantime G/S, and hence the pressure-Coriolis term in (11), can have a wide range of values depending on the baroclinity and the efficiency of the previous convective mixing.

c. *Effects on turbulence structure*

In spite of the rapid changes in ABL properties in our runs, the time change terms in the turbulence budgets were small. In the turbulent kinetic energy (E) budget, for example, $\partial E/\partial t$ was generally no larger than a few percent of ϵ. We can also interpret this in terms of time scales. The time scale of the response of the turbulence to changing conditions is $\tau_t \approx E/\epsilon$ (Tennekes and Lumley, 1972); for our runs τ_t was of the order of 30 s at 4 m and 100–200 s at 32 m, much less than the time scale of the changes shown in Fig. 1. Thus our turbulence was able to respond very quickly to the changing flow conditions, and could be called quasi-steady.

Thus we can reasonably conclude that the turbulence was essentially in equilibrium with the mean wind and potential temperature gradients, and that the time changes in the turbulence were almost entirely due to changes in these gradients. Our next, and more difficult, question is whether these gradients (and hence the turbulence structure) are representative of a stable boundary layer in a more nearly steady state. Posed in terms of time scales, the question is: What is the time scale of the response of the mean wind and potential temperature gradients as the nocturnal boundary layer evolves?

In considering this question we take first the case

where the agency causing the boundary-layer evolution—the surface cooling rate—is constant in time. Further, we consider wind speeds sufficiently large and mean temperature and humidity gradients sufficiently small that radiative flux divergence within the ABL can be neglected. In a horizontally homogeneous, barotropic flow over a level surface the mean gradient fields evolve according to

$$\frac{\partial \Theta'}{\partial t} = -\overline{\theta w}'', \tag{12}$$

$$\frac{\partial}{\partial t} U' = -\overline{uw}'' + fV', \tag{13}$$

$$\frac{\partial}{\partial t} V' = -\overline{vw}'' - fU', \tag{14}$$

where a prime denotes $\partial/\partial z$. We consider first the response of Θ'. From (12) a time scale of its evolution is

$$\tau_{\Theta'} = -\Theta'/\overline{\theta w}''. \tag{15}$$

For estimation purposes, we take as representative values $\Theta' \approx \Delta\theta/h$, $-\overline{\theta w}'' \approx Q_0/h^2$, where $\Delta\Theta$ is the potential temperature change across the ABL. This gives

$$\tau_{\Theta'} \approx \frac{h\Delta\Theta}{Q_0} \tag{16}$$

and for values typical of our runs ($h \approx 100$ m, $\Delta\Theta \approx 2$ K, $Q_0 \approx 0.01$ K m s^{-1}), Eq. (16) gives $\tau_{\Theta'} \approx 6$ h.

A parallel analysis shows that the mean shear responds to changing friction with a time scale of order $h\Delta U/u_*^2$, and for typical values ($h \approx 100$ m, $\Delta U \approx 5$ m s^{-1}, $u_* \approx 0.15$ m s^{-1}) this gives $\tau_{\Theta'} \approx 6$ h. The Coriolis terms impose a time scale f^{-1} which for Minnesota is ~ 3 h.

The Minnesota situation was even more complex because the surface cooling rate tended to decrease with time; for example, the average rate at 1 m decreased from 3.7 K h^{-1} in run 5B1 to 2.3 K h^{-1} in run 5B2. Thus it also seems relevant to consider the time required for the influence of changed surface conditions to reach the upper levels of the ABL. In analogy with the corresponding problem in laminar flow, we take this time (τ_d) at a height z to be of order $z^2/\bar{K}$, where $\bar{K}$ is a representative eddy diffusivity for the layer between the surface and z. Because τ_d itself changes with time, we consider two extremes: a neutral state, as a model of conditions at transition, and a steady, stable state which can be approached much later. We take $z \approx 100$ m, and in the neutral limit where $K_m = ku_*z$, we take $\bar{K} \approx 0.2\, u_* z$. Fig. 1 shows that u_* was typically 0.3 m s^{-1} at transition; thus we have

$$\tau_d \approx \frac{z^2}{\bar{K}} \approx \frac{5z}{u_*} \approx 0.5 \text{ h} \quad \text{(neutral limit)}. \tag{17}$$

In the steady, stable limit we take $h \approx 100$ m, and estimate a time τ_d for diffusion to $z \approx h/2 \approx 50$ m. The Brost-Wyngaard (1978) results indicate that for the lower half of a steady, stable PBL a representative value of $\bar{K}$ is 0.01 $u_* h$. Using $u_* \approx 0.1$ m s^{-1}, typical of the values at the end of our runs, we find

$$\tau_d \approx \frac{z^2}{\bar{K}} \approx \frac{25h}{u_*} \approx 7 \text{ h} \quad \text{(stable limit)}. \tag{18}$$

In view of these time-scale calculations, it seems that the mean wind and potential temperature gradients in our runs were probably not in equilibrium with the surface conditions, but instead were still evolving. If so, the turbulence structure was also evolving, and there is a strong possibility that our results might not be representative of steady, stably stratified ABL's (such as can exist in warm air advection or in polar regions). The model results suggest, in particular, that our ϵ and N profiles and our value for the constant d in the expression (9) for the stable ABL depth might not be representative.

We should also mention that there is reason to believe that under strong stable stratification and away from the surface, length scales of energy-containing turbulent eddies are limited by the strength of the stratification (Weinstock, 1978; Brost and Wyngaard, 1978). In the models of Delage (1974) and Brost and Wyngaard (1978), for example, the length scales are taken as proportional to $l_B = E^{\frac{1}{2}}/\omega_B$, where $\omega_B = [(g/T)\Theta']^{\frac{1}{2}}$ is the Brunt-Väisälä frequency. By this reasoning, near the top of the stable ABL λ_m scales with l_B rather than with h, as our data seem to show. However, in our runs Θ' near the ABL top was rather small, possibly because the runs were made so soon after transition, and hence ω_B values near h were not as large as might be found in equilibrium cases. In addition, runs with larger h had smaller ω_B (the product $h\omega_B$ varied much less than h alone). Thus any l_B influence on λ_m in our data could well have been small and masked by the ω_B, h correlation.

5. Conclusions

The stable boundary layer observed shortly after the evening transition in Minnesota was far from stationary. Time variations in surface temperature, stress and heat flux indicate a layer evolving rapidly with time. While the turbulence structure was able to respond quickly to these changes, the mean wind and temperature fields could not and hence were

probably far out of equilibrium with the surface conditions.

Although the Minnesota site was unusually flat, the terrain slope was significant enough to influence the vertical structure of the mean winds. The Ekman spiral evolved abnormally in three of the five evenings, evidently primarily because of baroclinic and/or advective effects, but partly also because of the terrain slope.

Nevertheless, the turbulence data show remarkable order when plotted in coordinates appropriate to the stably stratified PBL. The structure in the lowest one-tenth of the boundary layer, as observed in the spectral and cospectral properties of various parameters, is in good agreement with the Kansas results. The extensions of these properties through the remaining nine-tenths of the layer point to a steady drop in intensity in all parameters as their peak wavelengths approach a value close to h. Reasonable as these trends may appear, we cannot be sure that the observed structure is really that of an equilibrium boundary layer. Observations over polar sites or in warm air advection, where the PBL can persist long enough to approach equilibrium, are needed to verify these results.

Acknowledgments. The authors are indebted to the staff of the Meteorological Research Unit, Cardington, for the preliminary analysis of the data. The assistance of R. Brost and B. Stankov in the map analysis is gratefully acknowledged. R. Brost also kindly provided additional model runs to compare with the Minnesota results. We are also grateful to W. Neff for his helpful comments on the manuscript, and to J. Trebing for skillfully typing it. This research was supported in part by the Atmospheric Research Section, National Science Foundation, under Grant ATM 77-08690.

REFERENCES

Arya, S. P. S., and J. C. Wyngaard, 1975: Effect of baroclinicity on wind profiles and the geostrophic drag law for the convective planetary boundary layer. *J. Atmos. Sci.*, **32**, 767–778.

Businger, J. A., and S. P. S. Arya, 1974: Height of the mixed layer in the stably stratified planetary boundary layer. *Advances in Geophysics*, Vol. 18a, Academic Press, 73–92.

——, J. C. Wyngaard, Y. Izumi and E. F. Bradley, 1971: Flux-profile relationships in the atmosphere surface layer. *J. Atmos. Sci.*, **28**, 181–189.

Brost, R. A., and J. C. Wyngaard, 1978: A model study of the stably stratified planetary boundary layer. *J. Atmos. Sci.*, **35**, 1427–1440.

Caughey, S. J., 1977: Boundary-layer turbulence spectra in stable conditions. *Bound.-Layer Meteor.*, **11**, 3–14.

——, and J. C. Kaimal, 1977: Vertical heat flux in the convective boundary layer. *Quart. J. Roy. Meteor. Soc.*, **103**, 811–815.

——, and C. J. Readings, 1975: An observation of waves and turbulence in the earth's boundary layer. *Bound.-Layer Meteor.*, **9**, 279–296.

——, and J. C. Wyngaard, 1979: The turbulence kinetic energy budget in convective conditions. *Quart. J. Roy. Meteor. Soc.*, **105**, 231–239.

Deardorff, J. W., 1973a: An explanation of anomalously large Reynolds stresses within the convective planetary boundary layer. *J. Atmos. Sci.*, **30**, 1070–1076.

——, 1973b: Three-dimensional numerical modeling of the planetary boundary layer. *Workshop on Micrometeorology*, Amer. Meteor. Soc., 271–311.

——, 1974a: Three-dimensional numerical study of the height and mean structure of a heated planetary boundary layer. *Bound.-Layer Meteor.*, **7**, 81–106.

——, 1974b: Three-dimensional numerical study of turbulence in an entraining mixed layer. *Bound.-Layer Meteor.*, **7**, 199–226.

Delage, Y., 1974: A numerical study of the nocturnal atmospheric boundary layer. *Quart. J. Roy. Meteor. Soc.*, **100**, 351–364.

Jensen, N. O., and D. H. Lenschow, 1978: An observational investigation of penetrative convection. *J. Atmos. Sci.*, **35**, 1924–1933.

Kaimal, J. C., 1973: Turbulence spectra, length scales and structure parameters in the stable boundary layer. *Bound.-Layer Meteor.*, **4**, 289–309.

——, 1978: Horizontal velocity spectra in an unstable surface layer. *J. Atmos. Sci.*, **35**, 18–24.

——, J. C. Wyngaard, Y. Izumi and O. R. Coté, 1972: Spectral characteristics of surface layer turbulence. *Quart. J. Roy. Meteor. Soc.*, **98**, 563–589.

——, ——, D. A. Haugen, O. R. Coté, Y. Izumi, S. J. Caughey and C. J. Readings, 1976: Turbulence structure in the convective boundary layer. *J. Atmos. Sci.*, **33**, 2152–2169.

Lumley, J. L., and H. A. Panofsky, 1964: *The Structure of Atmospheric Turbulence.* Interscience, 239 pp.

Neumann, J., 1977: On the rotation rate of the direction of the sea and land breezes. *J. Atmos. Sci.*, **34**, 1913–1917.

Panofsky, H. A., 1978: Matching in the convective planetary boundary layer. *J. Atmos. Sci.*, **35**, 272–276.

——, H. Tennekes, D. H. Lenschow and J. C. Wyngaard, 1977: The characteristics of turbulent velocity components in the surface layer under convective conditions. *Bound.-Layer Meteor.*, **11**, 355–361.

Readings, C. J., D. A. Haugen and J. C. Kaimal, 1974: The 1973 Minnesota atmospheric boundary layer experiment. *Weather*, **29**, 309–312.

Tennekes, H., and J. L. Lumley, 1972: *A First Course in Turbulence.* The MIT Press, 287 pp.

Weinstock, J., 1978: Vertical turbulent diffusion in a stably stratified fluid. *J. Atmos. Sci.*, **35**, 1022–1027.

Wyngaard, J. C., 1975: Modeling the planetary boundary layer—extension to the stable case. *Bound.-Layer Meteor.*, **9**, 441–460.

——, and O. R. Coté, 1971: The budgets of turbulent kinetic energy and temperature variance in the atmospheric surface layer. *J. Atmos. Sci.*, **28**, 190–201.

Zilitinkevich, S. S., 1972: On the determination of the height of the Ekman boundary layer. *Bound.-Layer Meteor.*, **3**, 141–145.